Chiral Recognition by Resorcin[4]arene Receptors: Intrinsic Kinetics and Dynamics

Andrea Tafi,[a] Bruno Botta,[b] Maurizio Botta,[a] Giuliano Delle Monache,[c] Antonello Filippi,[b] and Maurizio Speranza*[b]

Abstract: Molecular recognition of representative amino acids (A) by a chiral amido[4]resorcinarene receptor ($\mathbf{1_L}$) was investigated in the gas phase by ESI-FT-ICR mass spectrometry. The ligand displacement reaction between noncovalent diastereomeric $[\mathbf{1_L}\cdot H\cdot A]^+$ complexes and the 2-aminobutane enantiomers (B) exhibits a distinct enantioselectivity with regard to both the leaving amino acid A and the amine reactant B. The emerging selectivity picture, discussed in the light of molecular mechanics and molecular dynamics calculations, points to chiral recognition by $\mathbf{1_L}$, as determined by the effects of the host asymmetric frame on the structure, stability, and rearrangement dynamics of the diastereomeric $[\mathbf{1_L}\cdot H\cdot A]^+$ complexes and the orientation of the amine reactant B in encounters with $[\mathbf{1_L}\cdot H\cdot A]^+$. The results contribute to the development of a dynamic model of chiral recognition of biomolecules by enzyme mimics in the unsolvated state.

Keywords: enantioselectivity · gas-phase kinetics · host–guest systems · mass spectrometry · molecular dynamics

Introduction

The remarkable catalytic proficiency and exceptional selectivity of enzymes towards biomolecules are ascribed to a combination of 1) shape-specific intermolecular interactions between functionalities located on the host–guest complementary surfaces, which severely limit their translational and (overall) rotational motion;[1] and 2) rate acceleration due to partial desolvation of the functionalities themselves in the host cavity.[2] Thus, understanding enzymatic catalysis requires the adoption of tailor-made simplified host–guest models and the comprehension of the intrinsic factors determining their behavior in the absence of solvation.

Calixarenes, long recognized as potential enzyme mimics,[3–12] are concave macrocyclic receptors, formed by the condensation of phenols and formaldehyde. Some of them are characterized by a very flexible cavity-shaped architecture due to the presence of suitably located side chains (pendants). The great majority of studies on calixarenes was carried out in solution and concerned their ability to selectively trap metal cations and transport them through liquid membranes.[3–14] Much attention has also been paid to the ability of calixarenes,[15–20] mostly tetrameric calix[4]arenes,[4,10–12] to discriminate biomolecules, for example, amino acids.[21–23]

Biomolecular recognition by unsolvated calixarenes[24–30] has been much less investigated. To date, only two very recent gas-phase studies can be found in the literature: 1) A gas-phase study on the displacement of several amino acids from the chiral amido[4]resorcinarene $\mathbf{1_L}$ (Figure 1) carried out by us using an electrospray-ionization Fourier-transform ion cyclotron resonance (ESI-FT-ICR) mass spectrometer,[31] and 2) a study by Lebrilla et al. on the ability of some achiral calix[6]arenes and calix[4]arenes to form inclusion complexes with natural amino acids under the conditions of matrix-assisted laser desorption ionization (MALDI).[32]

The molecular asymmetry of $\mathbf{1_L}$ is due to the four axial pendants containing the chiral L-valine group. In our ESI-FT-ICR study,[31] we found that the efficiency of the gas-phase exchange reaction between the proton-bonded com-

[a] Prof. A. Tafi, Prof. M. Botta
Dipartimento Farmaco Chimico Tecnologico
Università di Siena, 53100 Siena (Italy)

[b] Prof. B. Botta, Dr. A. Filippi, Prof. M. Speranza
Dipartimento degli Studi di Chimica e Tecnologia delle Sostanze Biologicamente Attive
Università"La Sapienza", 00185 Roma (Italy)
Fax: (+39)-06-49913602
E-mail: maurizio.speranza@uniroma1.it

[c] Dr. G. Delle Monache
Istituto Chimica del Riconoscimento Molecolare
Università Cattolica del Sacro Cuore, 00168 Roma (Italy)

Supporting information for this article is available on the WWW under http://www.chemeurj.org/ or from the author: Ion abundances and kinetic plots of the gas-phase reaction between $[\mathbf{1_L}\cdot H\cdot A]^+$ (A = none, Ala, Pro, Pip, and Ser) and B. Partial atomic charges used in the docking and MD simulations.

DOI: 10.1002/chem.200305772

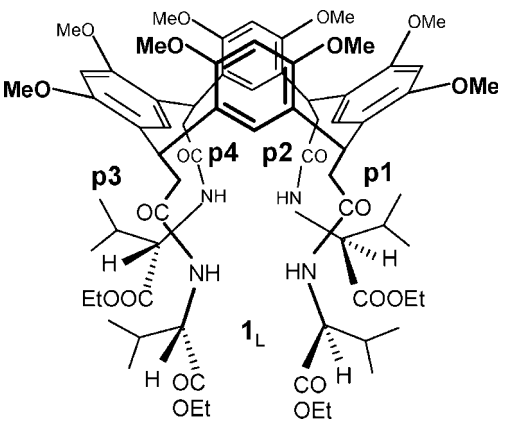

Figure 1. Schematic structure of the flattened-cone conformer of $\mathbf{1_L}$.

plexes $[\mathbf{1_L}\cdot H\cdot A]^+$ (A = D- and L-alanine, D- and L-serine) and (*S*)-(+)- and (*R*)-(−)-2-butylamine (B) [Eq. (1)] is appreciably affected by the configuration of both A and B.

$$[\mathbf{1_L}\cdot H\cdot A]^+ + B \rightarrow [\mathbf{1_L}\cdot H\cdot B]^+ + A \qquad (1)$$

With the aim of assessing the intrinsic factors determining the observed enantioselectivity, we extended the investigation to representative natural and nonnatural amino acids A with widely differing structures and basicities, such as alanine (Ala), leucine (Leu), proline (Pro), pipecolinic acid (Pip), serine (Ser), and 3,4-dihydroxyphenylalanine (DOPA). The relevant kinetic results are discussed in the light of molecular mechanics (MM) calculations and molecular dynamics (MD) simulations.

Abstract in Italian: *La spettrometria di massa ESI-FT-ICR è stata impiegata per lo studio del riconoscimento chirale di alcuni amminoacidi rappresentativi (A) da parte di un ammido[4]resorcinarene chirale (**1**$_L$). La reazione di rilascio dell'amminoacido A dai complessi diastereomerici non covalenti $[\mathbf{1}_L\cdot H\cdot A]^+$ a seguito dell'attacco degli enantiomeri del 2-amminobutano (B) mostra una distinta enantioselettività sia per quanto riguarda la molecola uscente A che per quanto riguarda il reagente B. Il quadro di reattività ottenuto, discusso alla luce di calcoli di meccanica e dinamica molecolare, indica che il riconoscimento chirale da parte di **1**$_L$ è determinato dall'effetto della struttura asimmetrica dell' ammido[4]resorcinarene sulla struttura, la stabilità, e la dinamica di riarrangiamento dei suoi complessi diastereomerici $[\mathbf{1}_L\cdot H\cdot A]^+$ e dall' orientamento dell'ammina reagente B nel complesso di collisione con $[\mathbf{1}_L\cdot H\cdot A]^+$. I risultati ottenuti contribuiscono allo sviluppo di un modello dinamico per il riconoscimento chirale di biomolecole da parte di enzimi artificiali allo stato non solvatato.*

Materials and Methods

Materials: Enantiomerically pure $\mathbf{1_L}$, in the flattened-cone conformation, was synthesized and purified according to established procedures.[33] The D and L enantiomers of the amino acids A were provided by Aldrich Co. and used without further purification. The same source provided the (*R*)-(−) (B_R) and (*S*)-(+) (B_S) enantiomers of 2-butylamine, which were purified in a vacuum manifold in several freeze–thaw cycles.

FT-ICR experiments: The experiments were performed at room temperature in an APEX 47e FT-ICR mass spectrometer equipped with an ESI source (Bruker Spectrospin) and a resonance cell ("infinity cell") situated between the poles of a superconducting magnet (4.7 T). Stock solutions of $\mathbf{1_L}$ (1×10^{-5} M) in H_2O/CH_3OH (1/3) containing a fivefold excess of the appropriate amino acid A were electrosprayed through a heated capillary (130 °C) into the external source of the FT-ICR mass spectrometer. The resulting ions were transferred into the resonance cell by a system of potentials and lenses and quenched by collisions with methane pulsed into the cell through a magnetic valve. Abundant signals, corresponding to the natural isotopomers of the proton-bound complex $[\mathbf{1_L}\cdot H\cdot A]^+$, were monitored and isolated by broadband ejection of the accompanying ions. The $[\mathbf{1_L}\cdot H\cdot A]^+$ family was then allowed to react with the chiral amine B present in the cell at a fixed pressure that ranged from 1×10^{-8} to 1×10^{-7} mbar, depending on its reactivity. Accurate measurement of the pressure of B in the resonance cell necessitates the use of an ion gauge whose sensitivity is dependent on the nature of the chemical species. The ionization gauge reading was corrected by first determining the rate constant of the reaction between the CH_4^+ radical cation and CH_4 in the FT-ICR instrument at a given nominal methane pressure and then by comparing the obtained result with the average value of reported rate constants for this process (1.13×10^{-9} cm^{3}molecule^{-1}s^{-1}).[34] Subsequently, the correction factor needed for amine B can be estimated by a method based on a linear dependence of the response of the ionization gauge with the polarizability of the base in question.[35]

When $[\mathbf{1_L}\cdot H\cdot A]^+$ is introduced in the resonance cell containing the chiral amine B at constant pressure, the exchange reaction (1) exclusively takes place. The appearance of the exchanged product $[\mathbf{1_L}\cdot H\cdot B]^+$ was monitored as a function of time *t*. If *I* is the intensity of complex $[\mathbf{1_L}\cdot H\cdot A]^+$ at delay time *t* and I_0 is the sum of the intensities of $[\mathbf{1_L}\cdot H\cdot A]^+$ and $[\mathbf{1_L}\cdot H\cdot B]^+$, linear $\ln(I/I_0)$ versus *t* plots were obtained for all systems investigated, except those with A = DOPA. Their good linearity (correlation coefficient $r^2 > 0.990$) confirms the view that the $[\mathbf{1_L}\cdot H\cdot A]^+$ complexes were collisionally thermalized by methane before they reacted with B. The rate constants *k* of reaction (1) were obtained from the slopes of the relevant linear $\ln(I/I_0)$ versus *t* plots. The corresponding second-order rate constants *k* are calculated from the ratio between the slope of the first-order plots and the B pressure. Their values, compared with the relevant collision rate constants k_{coll}, estimated according to Su's trajectory calculation method,[36] provides directly the efficiency of the reaction ($eff = k/k_{coll}$).

Docking and molecular dynamics calculations: All calculations were carried out on a SGI-Octane workstation. Molecular mechanics (MM) calculations (docking) and molecular dynamics simulations (MD) were performed with the AMBER* force field as implemented in MacroModel 5.5.[37] The extended nonbonded cutoff protocol of MacroModel was applied, and the calculations were performed in the gas phase with the constant-dielectric treatment (dielectric constant $\varepsilon = 1.0$). Partial atomic charges to be used in the docking and MD simulations were obtained by quantomechanics calculations performed with the semiempirical program MOPAC, distributed by Accelrys Inc., using the AM1–Mulliken method. The final charges used in this study are specified in the last column of the four Cartesian-coordinate structures enclosed as Supporting Information (.pdb format generated by InsightII), which describe a low-energy conformation of each compound.

With the aim of gathering some structural information on the proton-bound $[\mathbf{1_L}\cdot H\cdot A]^+$ complexes, two kinds of computational methodologies were employed: 1) The statistical Monte Carlo Multiple Minimum (MCMM) conformational search of A and $[\mathbf{1_L}\cdot H]^+$, coupled with random rototranslations of the A guest relative to the $[\mathbf{1_L}\cdot H]^+$ host standing still in the 3D space (MOLS command; MCMM/MOLS docking); and 2) Constant-temperature MD runs. Although MCMM/MOLS is indeed a

well described and validated docking protocol,[38] we are nevertheless aware that the number of rotatable bonds moved in each MCMM/MOLS run is well over the maximum allowed to guarantee exhaustive searches. In our opinion, this problem can be solved by combining docking studies with MD simulations to ensure a complete and reasonably homogeneous sampling of the whole potential energy hypersurface of our systems. Each MCMM/MOLS docking run was made up of 10000 steps. With A = Ala, a total of 22 torsional degrees of freedom were analyzed, while with A = Ser and DOPA the number of rotatable bonds was 24 and 26, respectively. In the docking calculations, the rototranslations of A with respect to $\mathbf{1}_L$ were limited by the maximum values of 180° for the rotational angle and of 5, 10, or 15 Å (changeable value) for the translational movement. At the same time, a randomly variable number of rotatable bonds of the side chains of $\mathbf{1}_L$ (the flexibility of the resorcarene skeleton was not directly sampled)[33] and A, ranging from 2 to $N-1$, where N is the overall number of variable torsion angles defined in the command file, was subjected to random step variations in the range 60–180°. Energy minimizations were performed by using the truncated Newton conjugate gradient (TNCG) procedure and were terminated when the rms energy gradient fell below 10 J mol^{-1} Å^{-1}. To eliminate duplicate conformations, a comparison was performed on the heavy atoms, whereby 1.0 Å was taken as the maximum allowable separation between couples of corresponding atoms after superimposition. All the conformers were saved that differed from the global minimum-energy conformation by no more than 50 kJ mol^{-1}. The overall conformation of each output docking geometry was classified by the values taken by ad hoc defined structural descriptors (SD).

The intermolecular out-of-plane bending shown in Figure 2 (left) for A = Ser was used to classify the output MCMM/MOLS docking geometries and to graph MD simulations. It was defined by picking four atoms as

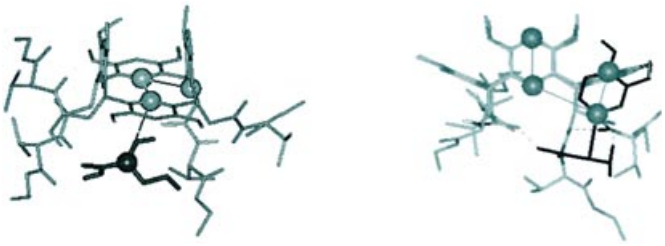

Figure 2. Left: Structural descriptor (SD) defined to classify the output MCMM/MOLS docking geometries and to graph MD simulations for $[\mathbf{1}_L\cdot H\cdot A]^+$ (A = Ala, Ser). Right: Structural descriptor (SD) defined to classify the output MCMM/MOLS docking geometries and to graph MD simulations for $[\mathbf{1}_L\cdot H\cdot A]^+$ (A = DOPA).

follows: taking C2 to be the carbon atom bearing the protonated side chain, the four designated atoms were, in sequential order, C28, C25, C27 for the host and the chiral carbon atom for the guest. The consequence of this choice is that SD values centered around 0° correspond to an external lower rim location of A in proximity to the protonated pendant of the host (henceforth denoted as *ext*). Values around −90° suggest a lower-rim location of the guest, among the pendants of the hosting resorcin[4]arene (henceforth denoted as *down*), and values of +90° its location in the achiral upper-rim cavity (henceforth denoted as *up*). Another structural descriptor, based on the intermolecular improper dihedral angle shown in Figure 2 (right), was defined to graph the MD/MC simulations of the $[\mathbf{1}_L\cdot H\cdot A]^+$ (A = DOPA) complexes. As for the SD of Figure 2 (left), SD values centered around 0°, −90°, and +90° correspond respectively to location of DOPA at external (*ext*), lower (*down*), and upper (*up*) sides of the hosting resorcin[4]arene.

Constant-temperature MD simulations with generation of the canonical ensemble were performed at 300 K. Coupling between the temperature bath and the molecules was updated every 0.2 ps. The equilibration period was 50 ps for every run, while the total simulation time was varied from 4 to 20 ns, depending on the target of the different simulations. During each trajectory, irrespective of its length, 5000 structures (frames) were sampled at regular intervals throughout the time course. Each recognition simulation (both docking and molecular dynamics) was repeated a few times, starting from different arbitrary geometries to produce a complete sampling of the whole potential energy hypersurface of the selected $[\mathbf{1}\cdot H\cdot A]^+$ systems. The convergence of the results guarantees the completeness of the study.

Results and Discussion

FT-ICR experiments: The pseudo-first-order rate constant of reaction (1) was obtained from the slopes of the relevant $\ln(I/I_0)$ versus t plots, where I is the intensity of complex $[\mathbf{1}_L\cdot H\cdot A]^+$ at the delay time t, and I_0 the sum of the intensities of $[\mathbf{1}_L\cdot H\cdot A]^+$ and $[\mathbf{1}_L\cdot H\cdot B]^+$. The corresponding second-order rate constants are denoted according to the configuration of the leaving amino acidic guest A (k_D or k_L) or to that of the incoming amine B (k_R or k_S). Enantioselectivity is defined in this discussion by the ratio $S_A = k_D/k_L$ when referring to the configuration of the amino acid A, or the ratio $S_B = k_R/k_S$ when referring to the configuration of the amine B. A value of $S_A > 1$ indicates that the amine B displaces the D enantiomer of A faster that the L enantiomer from the relevant diastereomeric $[\mathbf{1}_L\cdot H\cdot A_D]^+$ and $[\mathbf{1}_L\cdot H\cdot A_L]^+$ complexes. The opposite is true when $S_A < 1$. A value of $S_A = 1$ corresponds to equal displacement rates. Analogously, a value of $S_B > 1$ indicates that the displacement of the A guest from a given $[\mathbf{1}_L\cdot H\cdot A]^+$ diastereomer is faster with the *R* amine than with the *S* amine. Again, the opposite is true when $S_B < 1$. A value of $S_B = 1$ corresponds to equal displacement rates.

Figure 3 shows the pseudo-first-order kinetic plots for the displacement reaction (1) with $[\mathbf{1}_L\cdot H\cdot A]^+$ (A = Leu). Similar linear plots were obtained with A = Ala, Pro, Pip, and Ser

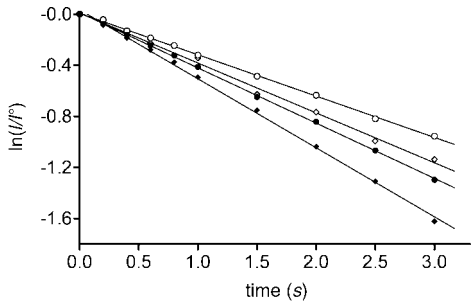

Figure 3. Kinetic plots for the gas-phase reaction between (*R*)-(−)- (circles) and (*S*)-(+)-2-butylamine (diamonds) ($P_B = 2.8\times10^{-8}$ mbar) and $[\mathbf{1}_L\cdot H\cdot A]^+$ (A = D-Leu (full symbols), L-Leu (open symbols)).

($r^2 > 0.993$; see Supporting Information). In contrast, irrespective of the configurations of A and B, the $\ln(I/I_0)$ versus t plots of $[\mathbf{1}_L\cdot H\cdot A]^+$ (A = DOPA) are not linear (Figure 4). The bimodal kinetics point to the presence of at least two isomeric structures in the initial diastereomeric $[\mathbf{1}_L\cdot H\cdot A_D]^+$ and $[\mathbf{1}_L\cdot H\cdot A_L]^+$ reactants. These isomeric structures react with the amine B at rates differing by a factor ranging from about 20 to greater than 30. At a B pressure of 4.9×10^{-8} mbar and reaction times longer than 1.2 s, the curves of Figure 4 become linear ($r^2 > 0.990$), that is, after 1.2 s only

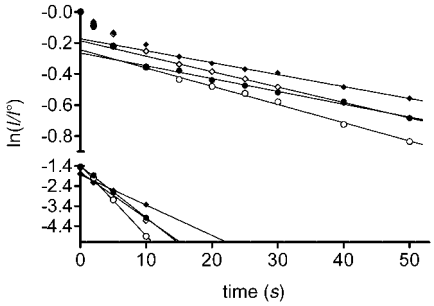

Figure 4. Kinetic plots for the gas-phase reaction between (*R*)-(−)- (circles) and (*S*)-(+)-2-butylamine (diamonds) ($P_B = 4.9 \times 10^{-8}$ mbar) and $[\mathbf{1_L}\cdot H\cdot A]^+$ (A = D-DOPA (full symbols), L-DOPA (open symbols)).

the less reactive isomer $([\mathbf{1_L}\cdot H\cdot A]^+)_{slow}$ is present. The time dependence of the more reactive fraction $([\mathbf{1_L}\cdot H\cdot A]^+)_{fast}$ can be inferred from the overall $[\mathbf{1_L}\cdot H\cdot A]^+$ decay after subtracting the first-order decay of the $([\mathbf{1_L}\cdot H\cdot A]^+)_{slow}$ fraction. The good linearity of the resulting curves ($r^2 = 0.976$), illustrated at the bottom of Figure 4, suggests that only a single isomer is present in the more reactive $([\mathbf{1_L}\cdot H\cdot A]^+)_{fast}$ fraction. The *y* intercepts of the linear extrapolations of Figure 4 provide an estimate of the relative distribution of the $([\mathbf{1_L}\cdot H\cdot A]^+)_{slow}$ and $([\mathbf{1_L}\cdot H\cdot A]^+)_{fast}$ isomers.

Thus, $([\mathbf{1_L}\cdot H\cdot A]^+)_{slow}/([\mathbf{1_L}\cdot H\cdot A]^+)_{fast} = (78\pm2)/(22\pm2)$ from the reaction with B_R. A similar distribution, namely, $([\mathbf{1_L}\cdot H\cdot A]^+)_{slow}/([\mathbf{1_L}\cdot H\cdot A]^+)_{fast} = (83\pm2)/(17\pm2)$, is obtained for the reaction with B_S.

The kinetics of the gas-phase displacement reaction (1) depend on the nature and the configuration of the amino acid guest and the configuration of the amine B (Table 1). Indeed, the efficiency of reaction (1) decreases with increasing proton affinity of the amino acid guest (PA(A), Table 1). In contrast, no simple correlations are found between PA(A) and the enantioselectivity factors S_A and S_B. Indeed, $S_A > 1$ for A = Ala and Leu, while the reverse is true for the other selected amino acids. In addition, the configuration of the amine B may ($S_A^R \neq S_A^S$ for Ala, Ser, and Pip) or may not affect the efficiency of reaction (1) ($S_A^R \approx S_A^S$ for Leu, DOPA, and Pro). Nor does a simple relationship exist between the configuration of the amine B and the enantioselectivity factors S_B. Thus, B_R reacts faster than B_S ($S_B > 1$) with all $[1_L\cdot H\cdot A]^+$ complexes, except those with A = Leu. A $S_B < 1$ value is also measured in the reaction with $[\mathbf{1_L}\cdot H\cdot A_L]^+$ (A_L = L-Ala and L-Ser).

The enantioselectivity picture emerging from Table 1 cannot be simply rationalized in terms of the relative stability of the diastereomeric $[\mathbf{1_L}\cdot H\cdot B]^+$ products of Equation (1). Indeed, ancillary FT-ICR kinetic measurements of the uptake of B_R and B_S ($P = 2.8\times10^{-8}$ mbar) by the protonated host $[\mathbf{1_L}\cdot H]^+$ [Eqs. (2)] provide the following rate constants: $k_{(2a)} = (5.2\pm0.1)\times10^{-11}$ and $k_{(2b)} = (3.4\pm0.1)\times10^{-11}$ cm^3 molecule^{-1} s^{-1}. Since the collision rate constant k_{coll}[36] for the same reactions can be estimated to be as large as 1.17×10^{-9} cm^3 molecule^{-1} s^{-1}, one can conclude that direct B uptake by $[\mathbf{1_L}\cdot H]^+$ [Eqs. (2)] is highly reversible. In this framework, the rate constant ratio ($k_{(2a)}/k_{(2b)} = 1.53\pm0.08$) would correspond approximately[39] to the $[\mathbf{1_L}\cdot H\cdot B_S]^+ \rightleftarrows [\mathbf{1_L}\cdot H\cdot B_R]^+$ equilibrium constant. Accordingly, $[\mathbf{1_L}\cdot H\cdot B_R]^+$ is more stable than the $[\mathbf{1_L}\cdot H\cdot B_S]^+$ by about 1 kJ mol^{-1} at 300 K.

$$[\mathbf{1_L}\cdot H]^+ + B_R \rightleftharpoons [\mathbf{1_L}\cdot H\cdot B_R]^+ \quad (2a)$$

$$[\mathbf{1_L}\cdot H]^+ + B_S \rightleftharpoons [\mathbf{1_L}\cdot H\cdot B_S]^+ \quad (2b)$$

Hence, the widely variable S_B factors (from 0.77 to 1.81), especially those below unity, cannot be explained in terms of the stability of the products of Equation (1). Indeed, if the exchange enantioselectivity reflects exclusively the $[\mathbf{1_L}\cdot H\cdot B_R]^+ > [\mathbf{1_L}\cdot H\cdot B_S]^+$ stability order, a constant value of $S_B = 1.5$ would be measured for all systems, in contrast to the experimental evidence. Most likely, the enantioselectivity factors reported in Table 1 are related to the effects of the resorcin[4]arene frame on the transition structures involved in the displacement reactions (1). Therefore, any attempt at rationalizing the enantioselectivity results of Table 1—in particular: 1) $S_A > 1$ for A = Ala; 2) $S_A < 1$ for A = Ser, DOPA; 3) the bimodal kinetics observed only with $[1_L\cdot H\cdot A]^+$ (A = DOPA); 4) the different S_B values for the fast and slow displacements of DOPA—should start from

Table 1. Rate constants of the displacement reactions (1).[a]

Amino acid (A)	PA(A) [kcal mol^{-1}]	(*R*)-(−)-$C_4H_9NH_2$ (B_R) k_R[a]	S_A^R	(*S*)-(+)-$C_4H_9NH_2$ (B_S) k_S[a]	S_A^S	S_B	Reaction efficiency k_R/k_{coll}	k_S/k_{coll}
D-Ala	215.5[42]	7.69±0.12	1.52±0.05	7.06±0.11	1.20±0.04	1.09±0.03	0.69	0.63
L-Ala		5.05±0.10		5.89±0.09		0.86±0.03	0.45	0.53
D-Ser	218.6[43]	4.59±0.06	0.67±0.02	3.70±0.06	0.49±0.01	1.24±0.05	0.41	0.34
L-Ser		6.87±0.05		7.56±0.06		0.91±0.02	0.62	0.68
D-Leu	218.6[42]	3.76±0.02	1.33±0.02	4.68±0.05	1.29±0.05	0.80±0.01	0.34	0.42
L-Leu		2.82±0.02		3.64±0.10		0.77±0.02	0.25	0.32
D-DOPA	221.0[b]	2.28±0.06	0.76±0.04	1.26±0.05	0.69±0.11	1.81±0.12	0.20	0.11
L-DOPA		3.00±0.09		1.82±0.20		1.65±0.24	0.27	0.16
D-DOPA		$0.07_3\pm0.00_8$	0.73±0.13	$0.06_4\pm0.00_8$	0.81±0.19	1.14±0.28	0.00_6	0.00_6
L-DOPA		$0.10_0\pm0.00_8$		$0.07_9\pm0.00_9$		1.27±0.25	0.00_9	0.00_7
D-Pro	224.9[44]	1.51±0.01	0.92±0.02	1.38±0.02	0.92±0.03	1.09±0.03	0.13	0.12
L-Pro		1.64±0.01		1.50±0.03		1.09±0.03	0.15	0.14
D-Pip	225.6[44]	$0.14_7\pm0.00_2$	0.91±0.02	$0.11_7\pm0.00_2$	0.74±0.02	1.26±0.04	0.01_3	0.01_0
L-Pip		$0.16_1\pm0.00_3$		$0.15_7\pm0.00_3$		1.02±0.04	0.01_4	0.01_4

[a] $k\times10^{-10}$ cm^3 molecule^{-1} s^{-1}. [b] Taken as equal to the PA of tyrosine.

the structural and energetic analysis of the relevant proton-bonded diastereomeric $[\mathbf{1_L}\cdot H\cdot A]^+$ reactants. This task was addressed by molecular mechanics (MM) calculations and molecular dynamics (MD) simulations.

Enantioselectivity in $[\mathbf{1_L}\cdot H\cdot A]^+$ (A = Ala) complexes: In a recent study,[40] Chimin and Houk used comprehensive MM calculations and MD simulations to assess the structures of hemicarcerands of neutral guests and to quantitatively evaluate their energetics. A similar quantitative estimate is not possible in the present study owing to the high flexibility of the $\mathbf{1_L}$ host, which greatly increases the number of conceivable structures of its stable adducts with the selected amino acids. Furthermore, the relatively large uncertainty associated with the computational approaches does not allow the quantitative reproduction of the small differences in free energy of activation (<2 kJ mol^{-1} at 300 K) inferred from the measured enantioselectivity values (Table 1). Instead, a qualitative structural investigation of the interactions between $\mathbf{1_L}$ and selected guests may be helpful in rationalizing the FT-ICR experimental results. As key examples, we selected those characterized by the highest measured enantioselectivity, namely, $[\mathbf{1_L}\cdot H\cdot A]^+$ (A = Ala) and $[\mathbf{1_L}\cdot H\cdot A]^+$ (A = Ser, DOPA), the former belonging to the $S_A > 1$ family (together with A = Leu) and the latter to the $S_A < 1$ family (together with A = Pro, Pip).

As pointed out in Materials and Methods, a complete and reasonably homogeneous sampling of the whole potential energy hypersurface of the selected $[\mathbf{1_L}\cdot H\cdot A]^+$ systems requires a combination of docking studies and MD simulations. The time evolution of the molecular motions of the host and guest moieties is expected to allow the system to move between conformations populated at room temperature by crossing over low energy barriers and by favoring large flat minima with respect to narrow ones, so as to provide a dynamic picture of the recognition process. Furthermore, energy minimizations in molecular mechanics (docking) give steric energies corresponding to enthalpies at 0 K. Therefore, to obtain average enthalpies at room temperature, more appropriate for large and flexible systems, a constant-temperature MD simulation is needed.

The nature of the proton-bound interaction in $[\mathbf{1_L}\cdot H\cdot A]^+$ was determined in a previous investigation on the basis of sustained off-resonance collision-induced decomposition (SORI-CID) experiments and MCMM simulations.[31] Accordingly, an energetically favored structure is obtained with the proton located on the oxygen atom of the **p2** amido group [the average enthalpy differences at 300 K amount to ca. 17 kJ mol^{-1} in favor of **p2**/**p3** (Figure 1)].

Figure 5 shows the results of docking calculations on diastereomeric $[\mathbf{1_L}\cdot H\cdot A]^+$ (A = Ala) complexes. The distribution of the relevant SD values (see Materials and Methods) as a function of the energy of output complexes (<20 kJ mol^{-1} over the global minimum) indicates that three regions of $[\mathbf{1_L}\cdot H]^+$ are best suited for hosting Ala: 1) among the four chiral pendants in correspondence with its chiral lower-rim cavity (*down*); 2) in the external position between the upper achiral and the lower chiral cavities in

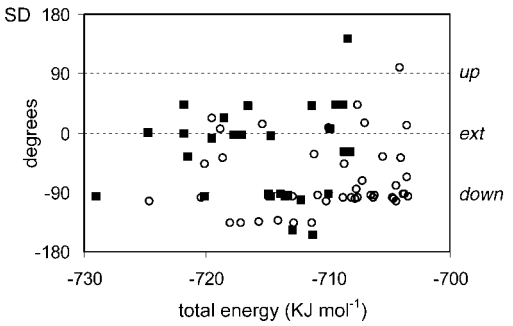

Figure 5. Docking of $[\mathbf{1_L}\cdot H\cdot A]^+$ (A = D-Ala (squares); L-Ala (circles)).

proximity to two adjacent pendants (*ext*); and 3) inside the achiral upper-rim cavity (*up*) with high steric energy.

Molecular dynamics runs up to 20 ns, performed at 300 K on low-energy docking geometries, reveal that both alanine enantiomers converge towards the *ext* region of the $[\mathbf{1}\cdot H]^+$ host, irrespective of the input geometry. An example of this behavior is illustrated in Figure 6 for A = L-Ala. These findings conform to the higher average potential energy values scaled to 300 K of its *down* and *up* regioisomers with $[\mathbf{1}\cdot H]^+$ relative to the *ext* isomer ($\Delta\Delta H_{300} = 0$ (*ext*), $+4$ (*down*), $+16$ kJ mol^{-1} (*up*)). In conclusion, MD simulations on low-energy $[\mathbf{1}\cdot H\cdot A]^+$ (A = Ala) docking geometries give equal average enthalpies for the diastereoisomeric inclusion complexes with A = L-Ala and A = D-Ala (results not shown) and point to *ext* as the thermodynamically most favored structures at room temperature (Figure 7). Therefore, the degenerate diastereomeric $[\mathbf{1}\cdot H\cdot A]^+$ (A = Ala) structures cannot be responsible by themselves for the pronounced enantioselectivity observed in their reaction with B ($S_R^A = 1.52 \pm 0.05$, $S_A^S = 1.20 \pm 0.04$; Table 1). This is instead attributable to the specific $[\mathbf{1_L}\cdot H\cdot A]^+$/B interactions in the relevant transition structures. In particular, the small effects of the configuration of B on the reaction kinetics ($S_B^D = 1.09 \pm 0.03$, $S_B^L = 0.86 \pm 0.03$) reveals that the amine B does not need to enter the chiral lower-rim cavity of the host to remove **Ala** from the *ext* position of $[\mathbf{1}\cdot H\cdot A]^+$ (A = **Ala**).

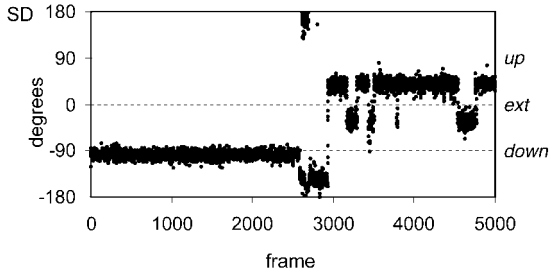

Figure 6. Molecular dynamics of $[\mathbf{1_L}\cdot H\cdot$L-Ala$]^+$.

Enantioselectivity in $[\mathbf{1_L}\cdot H\cdot A]^+$ (A = Ser) complexes: The computational protocol used for the $[\mathbf{1}\cdot H\cdot A]^+$ (A = Ala) systems was applied to the recognition of Ser and DOPA by $\mathbf{1_L}$. The opposite S_A enantioselectivity factors measured for

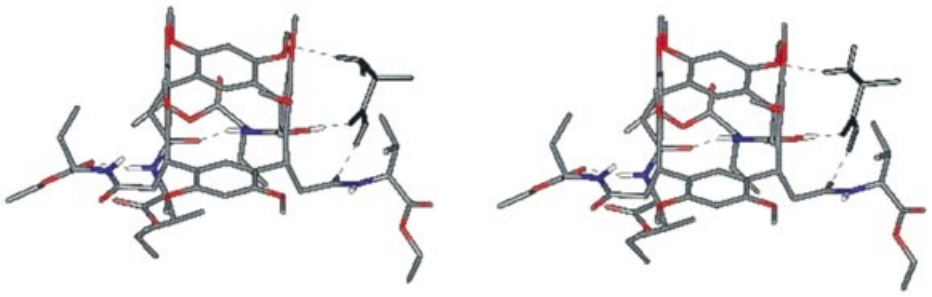

Figure 7. Three-quarter view of the fully minimized structure of the most representative *ext* $[\mathbf{1}_L\cdot H\cdot$L-Ala$]^+$ (left) and $[\mathbf{1}_L\cdot H\cdot$D-Ala$]^+$ (right) inclusion complexes. Hydrogen atoms bound to heteroatoms are shown, and hydrogen-bonding interactions are depicted as dashed lines.

$[\mathbf{1}_L\cdot H\cdot A]^+$ (A = Ser) and $[\mathbf{1}_L\cdot H\cdot A]^+$ (A = Ala) (Table 1) find a close correspondence in the computational analysis of the diastereomeric $[\mathbf{1}_L\cdot H\cdot A]^+$ (A = Ser) complexes, which reveals a picture that completely diverges from that of $[\mathbf{1}_L\cdot H\cdot A]^+$ (A = Ala). Indeed, the lowest-energy complexes, collected during the MCMM/MOLS calculations, exhibit some preference for the region of three-dimensional space enclosed by the four chiral pendants of $[\mathbf{1}_L\cdot H]^+$ (*down*), which is much more pronounced for D-Ser (squares in Figure 8) than for its L enantiomer (circles in Figure 8) and is highlighted by the squares falling at −90° within the 20 kJ mol^{-1} energy window above the global minimum.

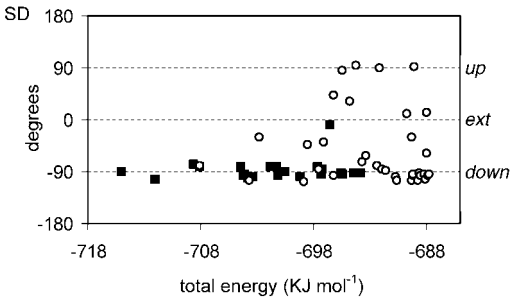

Figure 8. Docking of $[\mathbf{1}_L\cdot H\cdot A]^+$ (A = D-Ser (squares); L-Ser (circles)).

The observed correlation between the configuration of the guest and its regioselectivity towards the host is not completely unexpected. Indeed, the presence in the side chain of Ser of a hydroxy group, absent in the Ala analogues, may represent the third point of interaction with the $[\mathbf{1}_L\cdot H]^+$ chiral cavity (Easson–Steadman theory of three-point interactions).[41]

The presence of some SD values around 0° at higher steric energies in Figure 8 (circles) indicates that the *ext* region of $[\mathbf{1}_L\cdot H]^+$ might be accessible to the L-Ser guest. In the same figure, the SD values around +90° (circles in Figure 8), associated with only high-energy $[\mathbf{1}_L\cdot H\cdot A]^+$ (A = L-Ser) output structures (>13 kJ mol^{-1} above the global minimum), suggest that the *up* region of $[\mathbf{1}_L\cdot H]^+$ is hardly accessible to L-Ser. In this connection, it should be pointed out that the docking calculations did not assign any *up* geometries to $[\mathbf{1}_L\cdot H\cdot A]^+$ (A = D-Ser; squares in Figure 8), despite the achirality of the upper rim, which should equally accommodate the two enantiomers of Ser. This observation further demonstrates the impracticability of the sole MCMM/MOLS approach in exhaustively simulating recognition processes characterized by extremely uneven potential energy hypersurfaces and therefore the need of coupling it with MD to give a reliable description of the process.

Molecular dynamics runs up to 5 ns, carried out at 300 K on low-energy docking geometries to calculate average enthalpies of complexation (results not shown) confirm the docking picture and point to *down* and *ext* as the most favored hosting regions of $[\mathbf{1}_L\cdot H\cdot A]^+$ (A = Ser). The relevant average enthalpies of complexation ΔH_{av}, calculated from the difference between the average combined enthalpy of the two isolated components and that of the complex,[40] are estimated to be as large as 85 ($[\mathbf{1}_L\cdot H\cdot$D-Ser$]_+^{down}$), 60 ($[\mathbf{1}_L\cdot H\cdot$D-Ser$]_+^{ext}$), 61 ($[\mathbf{1}_L\cdot H\cdot$L-Ser$]_+^{down}$), and 59 kJ mol^{-1} ($[\mathbf{1}_L\cdot H\cdot$L-Ser$]_+^{ext}$). The results of these calculations confirm and clarify both the docking results and the MD simulations when the MD runs are extended to 20 ns (Figure 8 and Figure 9, respectively). Indeed, the *down* region of $[\mathbf{1}_L\cdot H]^+$ accommodates D-Ser much better than L-Ser ($\Delta\Delta H_{av} = (\Delta H_{av})_{D\text{-Ser}} - (\Delta H_{av})_{L\text{-Ser}} = 24$ kJ mol^{-1}). This significant stability difference is reflected in the docking and MD simulations, which indicate that D-Ser prefers to remain in the *down* position of the host (Figure 9a), whereas L-Ser may relocate to the almost degenerate *ext* region of $[\mathbf{1}_L\cdot H]^+$ (Figure 9b), probably driven by entropy factors.

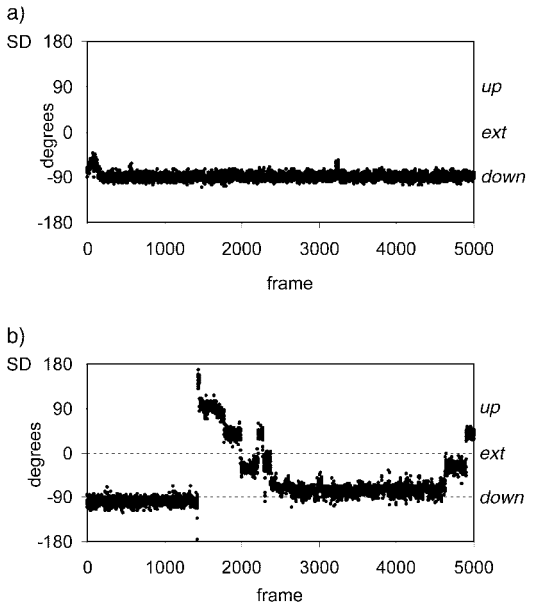

Figure 9. Molecular dynamics of $[\mathbf{1}_L\cdot H\cdot A]^+$ (A = D-Ser (a), L-Ser (b)).

The 24 kJ mol^{-1} difference in stability between the persistent $[\mathbf{1}_L\cdot H\cdot D\text{-Ser}]_+^{down}$ structure and the dynamically interconverting $[\mathbf{1}_L\cdot H\cdot D\text{-Ser}]_+^{ext}/[\mathbf{1}_L\cdot H\cdot L\text{-Ser}]_{+\,down}^{+}$ structures can account for the observed pronounced effect of the guest configuration on reaction (1) ($S_A^R = 0.67 \pm 0.02$, $S_A^S = 0.49 \pm 0.01$). However, this view may prove too simplistic when considering the largely different (and opposite) effect of the configuration of B measured in the reaction (S_B in Table 1). Indeed, as for $[\mathbf{1}\cdot H\cdot A]^+$ (A = Ala) ($S_B^L = 0.86 \pm 0.03$, $S_B^D = 1.09 \pm 0.03$), no significant B effect is measured with $[\mathbf{1}\cdot H\cdot A]^+$ (A = L-Ser) ($S_B^L = 0.91 \pm 0.02$). This coincidence points to a common displacement route for both $[\mathbf{1}\cdot H\cdot A]^+$ (A = L-Ser) and $[\mathbf{1}\cdot H\cdot A]^+$ (A = Ala), wherein the B amine can remove the amino acid guest from the *ext* position of the host without entering its chiral lower-rim cavity. In contrast, when amine B reacts with the persistent *down* regioisomer of $[\mathbf{1}\cdot H\cdot A]^+$ (A = D-Ser), a larger effect of the B configuration is observed ($S_B^D = 1.24 \pm 0.05$), which points to the involvement of a more congested, high-energy transition structure in which B partially enters the host chiral cavity to oust the D-serine guest. This view is supported by the smaller reaction efficiencies measured for the reaction on $[\mathbf{1}\cdot H\cdot A]^+$ (A = D-Ser) relative to those for $[\mathbf{1}\cdot H\cdot A]^+$ (A = L-Ser, Ala) (0.34–0.41 vs 0.45–0.69, Table 1).

Enantioselectivity in $[\mathbf{1}_L\cdot H\cdot A]^+$ (A = DOPA) complexes: The results of MCMM/MOLS calculations on a large number (several thousands) of diastereomeric systems yields a reasonable family of low-energy $[\mathbf{1}_L\cdot H\cdot A]^+$ (A = DOPA) output structures (< 20 kJ mol^{-1} above the global minimum), as shown in Figure 10. Although the distribution of the SD values over the total number of structures collected might suggest some incompleteness of the search on the D-DOPA systems, its analysis nevertheless is of some help, especially in the case of L-DOPA. Like with L-Ser, all three *down*, *up*, and *ext* regions of $[\mathbf{1}_L\cdot H]^+$ proved suitable for hosting the enantiomers of DOPA.

To overcome the intrinsic dimensional difficulty of the DOPA systems and to explore their configurational space more effectively than by Monte Carlo (MC) or MD, the mixed mode MD/MC of MacroModel was applied, which mixes both methodologies in a single simulation, while using the dynamics paradigm to obtain average enthalpies at room temperature. This approach is recognized to allow the crossing of large energy barriers by attempting MC variations of internal coordinates (variation of torsion angles, and rototranslations in our case) for every dynamics time step. Some 20 ps MD/MC runs were performed starting from low-energy output *down*, *ext*, and *up* docking geometries of both enantiomers of DOPA.

The MD/MC simulations starting from the global minimum of both diastereomeric

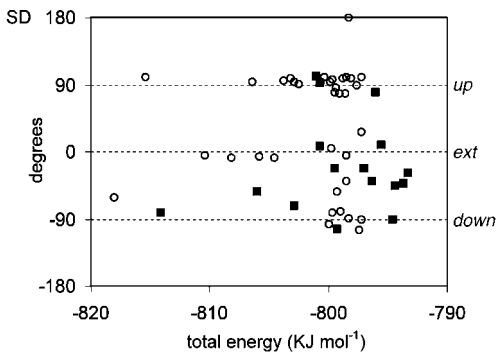

Figure 10. Docking of $[\mathbf{1}_L\cdot H\cdot A]^+$ (A = D-DOPA (squares), L-DOPA circles)).

$[\mathbf{1}\cdot H\cdot A]^+$ (A = DOPA) complexes suggest that the DOPA guest can be permanently trapped in the chiral lower rim of $[\mathbf{1}_L\cdot H]^+$ (the *down* region; Figure 11). As shown in Figure 12, in order to optimize the interaction with the guest, the pendants of $[\mathbf{1}\cdot H]^+$ adopt a preorganized "canyon-shaped" architecture due to the formation of a pair of stable hydrogen bonds between adjacent side chains **p3** and **p4**.

During the simulation, the phenyl ring of either L- or D-DOPA is firmly accommodated in the cleft by a stable network of intermolecular hydrogen bonds with the OH groups (interacting with the carbonyl oxygen atoms at **p1** and **p3**) and the acidic function (interacting with the protonated

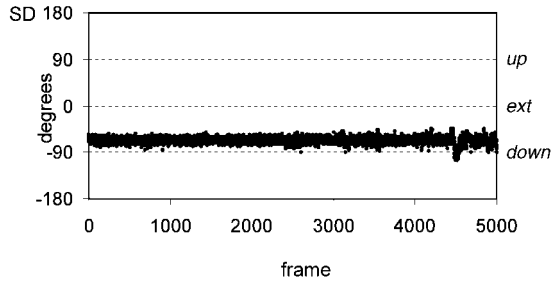

Figure 11. MD/MC simulations of the *down* regioisomer of $[\mathbf{1}_L\cdot H\cdot A]^+$ (A = D-DOPA). A similar behavior was observed for $[\mathbf{1}_L\cdot H\cdot A]^+$ (A = L-DOPA).

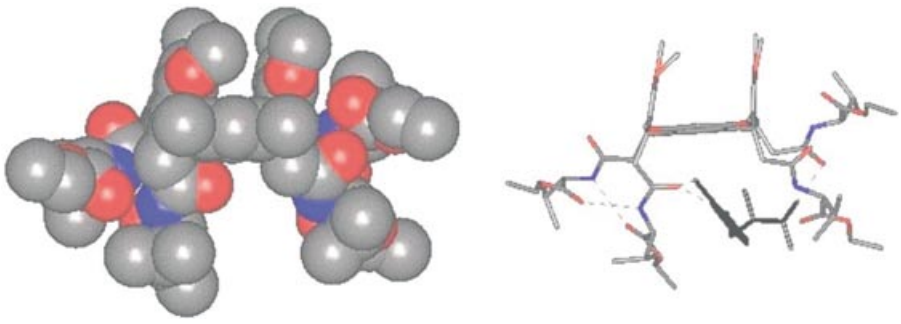

Figure 12. Right: side view of the global minimum structure of the $[\mathbf{1}_L\cdot H\cdot D\text{-DOPA}]^+$ *down* complex (For the sake of simplicity hydrogen atoms are not shown, while hydrogen-bonding interactions are depicted as dashed lines). Left: "canyon-shaped" architecture adopted by the hosting partner (CPK model of $[\mathbf{1}_L\cdot H]^+$ extracted from the whole complex) to host D-DOPA among the four chiral pendants.

amide at **p2**), but not with the amino group. The diastereomeric *down* structures exhibit similar average enthalpies, calculated at 300 K, although their geometries are rather different. For instance, in the complex with D-DOPA, the NH_2 group of the guest is directed towards one of the $[\mathbf{1}\cdot H]^+$ aromatic rings, while the same groups are parallel in the complex with L-DOPA (Figure 13).

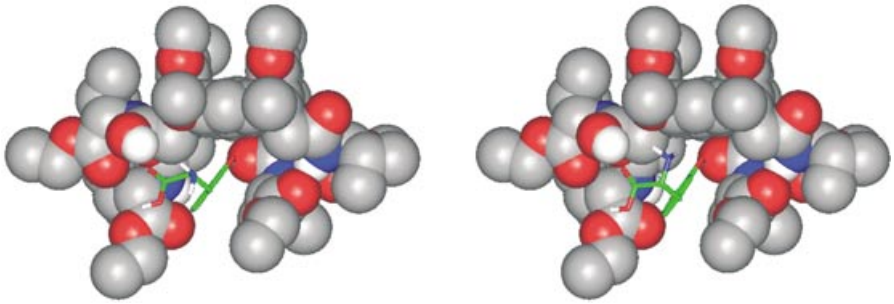

Figure 13. Three-quarter view of the fully minimized structure of the most representative *down* $[\mathbf{1_L}\cdot H\cdot$L-DOPA$]^+$ (left) and $[\mathbf{1_L}\cdot H\cdot$D-DOPA$]^+$ (right) inclusion complexes. Hydrogen atoms bound to heteroatoms are shown, and hydrogen-bonding interactions are depicted as dotted lines.

The SD values from MD/MC simulations indicate that, irrespective of its configuration, the DOPA guest can be permanently trapped in the achiral upper rim of $[\mathbf{1_L}\cdot H]^+$ (the *up* region) as well (Figure 14). The average enthalpies of the

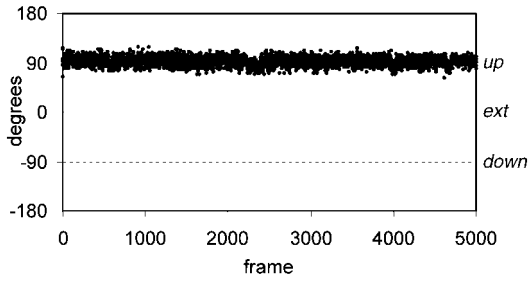

Figure 14. MD/MC simulations of the *up* regioisomer of $[\mathbf{1_L}\cdot H\cdot A]^+$ (A = D-DOPA). A similar behavior was observed for $[\mathbf{1_L}\cdot H\cdot A]^+$ (A = L-DOPA).

diastereomeric *up* structures, calculated at 300 K, are very similar and about 20 kJ mol^{-1} higher than those of the *down* regioisomers.

In contrast, the MD/MC simulations starting from *ext* geometries exhibit significant differences. Accordingly, D-DOPA is better hosted than L-DOPA by $[\mathbf{1_L}\cdot H]^+$ (by 10 kJ mol^{-1}) and moves during the simulations towards the lower rim of $[\mathbf{1_L}\cdot H]^+$ (the *down* region; Figure 15).

By this movement, the two phenolic OH groups of D-DOPA can form hydrogen bonds with the polar amido groups of $[\mathbf{1_L}\cdot H]^+$ (Figure 16, top). In contrast, the L-DOPA guest permanently remains in the *ext* region of $[\mathbf{1_L}\cdot H]^+$ (Figure 16, bottom). The average enthalpy of the *ext* structures exceeds those of the relevant *up* and *down* regioisomers by 40 kJ mol^{-1}.

The MC/MD simulations pointing to the persistency of the chiral *down* and achiral *up* regioisomers of $[\mathbf{1_L}\cdot H\cdot A]^+$ (A = DOPA), are consistent with the bimodal kinetics of Figure 4. Owing to the 20 kJ mol^{-1} stability difference, the *down* structure is associated with the most abundant $([\mathbf{1_L}\cdot H\cdot A]^+)_{slow}$ fraction (ca. 80%), and the *up* structure with the less abundant $([\mathbf{1_L}\cdot H\cdot A]^+)_{fast}$ component (ca. 20%). This assignment is consistent with the relevant S_B factors as well (Table 1). Note that the B-induced DOPA loss from the *achiral up* region of $[\mathbf{1_L}\cdot H]^+$ (i.e., in $([\mathbf{1_L}\cdot H\cdot A]^+)_{fast}$) is accompanied by high S_B values ($S_B^D = 1.81 \pm 0.12$, $S_B^L = 1.65 \pm 0.24$), not far from those measured in the direct uptake of B by $[\mathbf{1}\cdot H]^+$ ($k_R/k_S = 1.53 \pm 0.08$). This coincidence suggests that the B amine must be completely embodied into the asymmetric lower-rim cavity of $([\mathbf{1_L}\cdot H\cdot A]^+)_{fast}$ (A = DOPA) to push away the guest from its *up* position (a "backside" displacement). In contrast, comparatively small S_B values ($S_B^D = 1.14 \pm 0.28$, $S_B^L = 1.27 \pm 0.25$) are associated with B-induced DOPA loss from the *chiral down* region of $[\mathbf{1}\cdot H\cdot A]^+$ (A = DOPA), that is, in $([\mathbf{1_L}\cdot H\cdot A]^+)_{slow}$). A similar S_B value is observed in the same reaction with $[\mathbf{1}\cdot H\cdot A]^+$ (A = D-Ser) ($S_B^D = 1.24 \pm 0.05$). Again, this coincidence indicates that the B amine can remove the amino acid guest located inside the asymmetric lower-rim cavity of

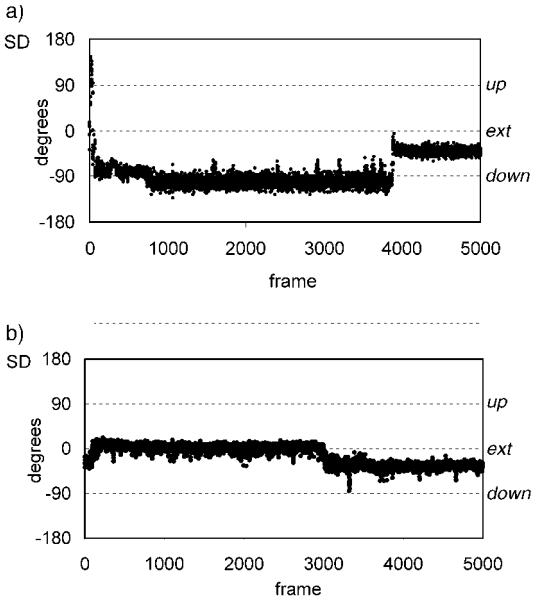

Figure 15. MD/MC simulations of the *ext* regioisomers of $[\mathbf{1_L}\cdot H\cdot A]^+$ (A = D-DOPA (a), L-DOPA (b)).

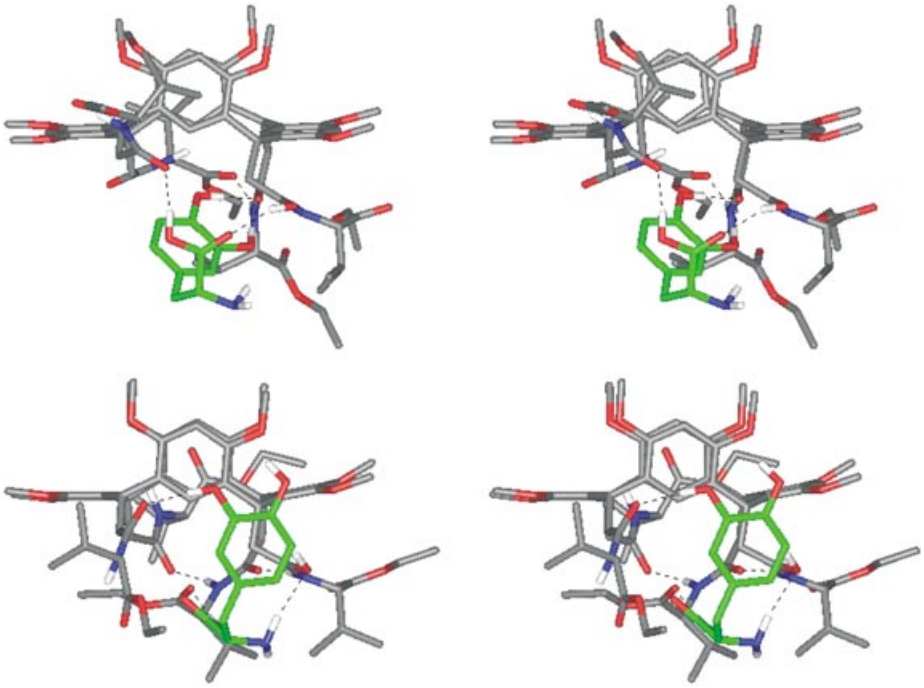

Figure 16. Side view (crossed stereoview) of the fully minimized structures of the most representative *ext* $[\mathbf{1}_L\cdot H\cdot D\text{-DOPA}]^+$ (top) and $[\mathbf{1}_L\cdot H\cdot L\text{-DOPA}]^+$ (bottom) inclusion complexes. Hydrogen atoms bound to heteroatoms are shown, and hydrogen-bonding interactions are depicted as dashed lines. Carbon atoms of the host are colored gray, while green is used for the guest.

$([\mathbf{1}_L\cdot H\cdot A]^+)_{slow}$ (A = DOPA) only by partially entering the same cavity (a "frontside" displacement). In the relevant, highly congested transition structures, the B amine is not completely embodied into the host cavity, which therefore may only partially exert its asymmetry towards it.

Conclusion

The proton-bound complexes between the chiral amido[4]resorcinarene host $\mathbf{1}_L$ and representative amino acids A were allowed to react with the 2-aminobutane enantiomers B in the resonance cell of a ESI-FT-ICR instrument. A guest-exchange reaction was observed which exhibits a distinct enantioselectivity with regards to both the leaving amino acid A and the amine reactant B. The resulting selectivity picture has been discussed in the light of molecular mechanics and molecular dynamics calculations. Differences in exchange selectivities are attributed to the effects of the host asymmetric frame on the structure, stability, and rearrangement dynamics of the diastereomeric $[\mathbf{1}_L\cdot H\cdot A]^+$ complexes and the orientation of the amine reactant B in encounters with $[\mathbf{1}_L\cdot H\cdot A]^+$. The limited influence of the configuration of the A guest ($S_A = k_D/k_L$) or of amine B ($S_B = k_R/k_S$) on the exchange rate of $[\mathbf{1}_L\cdot H\cdot A]^+$ (A = Ala) is due to the attack of the amine on the guest located outside the host in the proximity of two adjacent pendants (*ext*). The $S_A < 1$ selectivity factors measured for $[\mathbf{1}_L\cdot H\cdot A]^+$ (A = Ser) are determined by the greater stability of $[\mathbf{1}_L\cdot H\cdot A]^+$ (A = D-Ser), in which the guest is located inside the chiral cavity of the host (the *down* region), relative to $[\mathbf{1}_L\cdot H\cdot A]^+$ (A = L-Ser), in which the guest moves between the degenerate *ext* and *down* positions. The comparatively large S_B selectivity factors measured for the *down* $[\mathbf{1}_L\cdot H\cdot A]^+$ (A = D-Ser) structure are attributed to "frontside" displacement of the amino acid by the amine, in which both are located inside the host cavity. The bimodal kinetics observed with $[\mathbf{1}_L\cdot H\cdot A]^+$ (A = DOPA) are due to the simultaneous formation of persistent *up* and *down* regioisomers. The large S_B selectivity factors measured for the *up* $[\mathbf{1}_L\cdot H\cdot A]^+$ (A = DOPA) structure, are attributed to the "backside" displacement of the amino acid by amine entirely embodied in the host cavity. Ligand-exchange dynamics similar to those proposed for the *down* $[\mathbf{1}_L\cdot H\cdot A]^+$ (A = D-Ser) structure account for the comparatively limited S_B selectivity factors measured for the *down* $[\mathbf{1}_L\cdot H\cdot A]^+$ (A = DOPA) structure. The studied cases demonstrate the importance of a dynamic model for chiral recognition of biomolecules by enzyme mimics in the unsolvated state.

Acknowledgement

Work supported by the Ministero dell'Istruzione dell'Università e della Ricerca (MIUR) and the Consiglio Nazionale delle Ricerche (CNR). M.S. and A.F. express their gratitude to F. Angelelli for technical assistance.

[1] M. I. Page, W. P. Jencks, *Proc. Natl. Acad. Sci. USA* **1971**, *68*, 1678–1683.
[2] F. Hollfelder, A. J. Kirby, D. S. Tawfik, *Nature* **1996**, *383*, 60–63; See also: F. Hollfelder, A. J. Kirby, D. S. Tawfik, *J. Org. Chem.* **2001**, *66*, 5866–5874.
[3] a) C. D. Gutsche, *Calixarenes in Monographs in Supramolecular Chemistry* (Ed: J. F. Stoddart), Royal Society of Chemistry, Cambridge, **1989**; b) C. D. Gutsche, *Calixarenes Revisited in Monographs in Supramolecular Chemistry* (Ed.: J. F. Stoddart), Royal Society of Chemistry, Cambridge, **1998**.
[4] *Topics in Inclusion Science*, *Vol. III*, *Calixarenes: A Versatile Class of Macrocyclic Compounds* (Eds.: J. Vicens, V. Böhmer), Kluwer Academic Publishers, Dordrect, **1991**.
[5] V. Böhmer, *Angew. Chem.* **1995**, 34, 785–818; *Angew. Chem. Int. Ed. Engl.* **1995**, *34*, 713–745.
[6] A. M. A. van Wageningen, W. Verboom, D. N. Reinhoudt, *Pure Appl. Chem.* **1996**, *68*, 1273–1277.
[7] A. Ikeda, S. Shinkai, *Chem. Rev.* **1997**, *97*, 1713–1734.
[8] *Calixarenes in Action* (Eds.: L. Mandolini, R. Ungaro), Imperial College Press, London, **2000**.
[9] Z. Asfari, V. Böhmer, J. Harrowfield, J. Vicens, *Calixarenes 2001*, Kluwer Academic Publishers, Dordrect, **2001**.

[10] J. M. Harrowfield, W. R. Richmond, A. N. Sobolev, A. H. White, *J. Chem. Soc. Perkin Trans. 2* **1994**, *1*, 5–9.
[11] R. Ludwig, *Fresenius J. Anal. Chem.* **2000**, *367*, 103–128.
[12] G. Arena, A. Contino, A. Magri, D. Sciotto, G. Spoto, A. Torrisi, *Ind. Eng. Chem. Res.* **2000**, *39*, 3605–3610.
[13] R. M. Izatt, R. T. Lamb, R. T. Hawkins, P. R. Brown, S. R. Izatt, J. J. Christensen, *J. Am. Chem. Soc.* **1983**, *105*, 1782–1785.
[14] R. M. Izatt, R. T. Hawkins, J. J. Christensen, S. R. Izatt, *J. Am. Chem. Soc.* **1985**, *107*, 63–66.
[15] I. S. Antipin, I. I. Stoikov, E. M. Pinkhassik, N. A. Fitseva, I. Stibor, A. I. Konovalov, *Tetrahedron Lett.* **1997**, *38*, 5865–5868.
[16] N. Douteau-Guevel, A. W. Coleman, J. P. Morel, N. Morel-Desrosiers, *J. Phys. Org. Chem.* **1998**, *11*, 693–696.
[17] N. Douteau-Guevel, A. W. Coleman, J. P. Morel, N. Morel-Desrosiers, *J. Chem. Soc. Perkin Trans. 2* **1999**, *3*, 629–634.
[18] G. Arena, A. Contino, F. G. Gulino, A. Magri, F. Sansone, D. Sciotto, R. Ungaro, *Tetrahedron Lett.* **1999**, *40*, 1597–1600.
[19] M. Selkti, A. Tomas, A. W. Coleman, N. Douteau-Guevel, I. Nicolis, F. Villain, C. de Rango, *Chem. Commun.* **2000**, *2*, 161–162.
[20] H. J. Buschmann, L. Mutihac, K. Jansen, *J. Inclusion Phenom. Macrocyclic Chem.* **2001**, *39*, 1–11.
[21] K. Araki, K. Inada, S. Shinkai, *Angew. Chem.* **1996**, *108*, 92–94; *Angew. Chem. Int. Ed. Engl.* **1996**, *35*, 72–74.
[22] Y. Kubo, S. Y. Maeda, S. Tokita, M. Kubo, *Nature* **1996**, *382*, 522–524.
[23] K. Ito, K. Atsushi, Y. Ohba, T. Sone, *Chem. Lett.* **1998**, *12*, 1221–1222.
[24] M. Vincenti, A. Irico, *Int. J. Mass Spectrom.* **2002**, *214*, 23–36, and references therein.
[25] T. M. Liang, K. K. Laali, M. Cordero, C. Wesdemiotis, *J. Chem. Res. Synop.* **1991**, 354–355.
[26] M. Makinen, P. Vainiotalo, M. Nissinen, K. Rissanen, *J. Am. Soc. Mass Spectrom.* **2003**, *14*, 143–151.
[27] M. Makinen, P. Vainiotalo, K. Rissanen, *J. Am. Soc. Mass Spectrom.* **2002**, *13*, 851–861.
[28] M. Vincenti, A. Irico, E. Dalcanale, *Adv. Mass Spectrom.* **1998**, *14*, Chaps. 7/129–7/150, and references therein.
[29] M. Vincenti, E. Dalcanale, *J. Chem. Soc. Perkin Trans. 2* **1995**, 1069–1076.
[30] J. M. J. Nuutinen, A. Irico, M. Vincenti, E. Dalcanale, J. M. H. Pakarinen, P. Vainiotalo, *J. Am. Chem. Soc.* **2000**, *122*, 10090–10100.
[31] B. Botta, M. Botta, A. Filippi, A. Tafi, G. Delle Monache, M. Speranza, *J. Am. Chem. Soc.* **2002**, *124*, 7658–7659.
[32] M. M. Stone, A. H. Franz, C. B. Lebrilla, *J. Am. Soc. Mass Spectrom.* **2002**, *13*, 964–974.
[33] B. Botta, G. Delle Monache, P. Salvatore, F. Gasparrini, C. Villani, M. Botta, F. Corelli, A. Tafi, E. Gacs-Baitz, A. Santini, C. F. Carvalho, D. Misiti, *J. Org. Chem.* **1997**, *62*, 932–938.
[34] Y. Ikezoe, S. Matsuoka, M. Takebe, A. A. Viggiano, *Gas-Phase Ion–Molecule reaction Rate Constants through 1986* , Maruzen Company, Ltd., Tokyo, **1987**.
[35] J. E. Bartmess, R. M. Georgiadis, *Vacuum* **1983**, *33*, 149.
[36] T. Su, *J. Chem. Phys.* **1988**, *88*, 4102–4103, 5355.
[37] F. Mohamadi, N. G. J. Richards, W. C. Guida, R. Liskamp, M. Lipton, C. Caufield, G. Chang, T. Hendrickson, W. C. Still, *J. Comput. Chem.* **1990**, *11*, 440–467.
[38] A. Tafi, A. van Amsick, F. Corelli, M. Crusco, K. E. Laumen, M. P. Schneider, M. Botta, *J. Org. Chem.* **2000**, *65*, 3659–3665.
[39] Strictly speaking, the used kinetic measurement of the stability scale of the diastereomeric $[\mathbf{1}_L \cdot H \cdot B_R]^+$ and $[\mathbf{1}_L \cdot H \cdot B_S]^+$ complexes is acceptable only by assuming no significant energy barrier in their backdissociation and the same energetics in their formation.
[40] S. Chimin, K. N. Houk, *J. Am. Chem. Soc.* **1996**, *118*, 8056–8070.
[41] C. B. Lebrilla, *Acc. Chem. Res.* **2001**, *34*, 653–661,and reference therein.
[42] P. B. Armentrout, *J. Am. Soc. Mass Spectrom.* **2000**, *11*, 371.
[43] http://webbook.nist.gov/chemistry/name-ser.html.
[44] A. F. Kuntz, A. W. Boynton, G. A. David, K. E. Colyer, J. C. Poutsma, *J. Am. Soc. Mass Spectrom.* **2002**, *13*, 72.

Received: December 3, 2003
Revised: April 23, 2004
Published online: July 7, 2004

